Acta Biochim Biophys Sin 2026, 58(10): 2366–2379
https://cstr.cn/32197.14.abbs.2026073
https://doi.org/10.3724/abbs.2026073
Original Article

Original Article

Vitamin C exerts a concentration-dependent dual effect on melanoma progression through the ERK-PTPN12-JAK2 axis

Caixia Zhang[1,†], Bingxue Chen[2,†], Hui Wang[3], Shuaishuai Xie[3], Yian Guan[4], Yingxiang Liu[5], Shiyu Ji[3], Weiwei Huang[3], and Zekun Guo[3,*]

[1]College of Veterinary Medicine, Northwest A&F University, Yangling 712100, China, [2]Shandong Provincial Key Laboratory of Animal Cells and Developmental Biology, School of Life Sciences, Shandong University, Qingdao 266237, China, [3]College of Life Sciences, Northwest A&F University, Yangling 712100, China, [4]Institute for Translational Brain Research, Fudan University, Shanghai 200433, China, and [5]Orthopedic Oncology Institute, Department of Orthopedic Surgery, Tangdu Hospital, Fourth Military Medical University, Xi'an 710000, China
[†]These authors contributed equally to this work.
*Correspondence address. E-mail: gzk@nwafu.edu.cn

Received 12 November 2025 Accepted 31 March 2026 Published 30 April 2026

Abstract

The role of vitamin C (Vc) in cancer therapy has been debated for decades. Notably, Vc has a concentration-dependent dual effect on malignant melanoma; however, the underlying molecular mechanism remains to be explored. In this study, we aim to investigate the mechanism underlying these opposing effects. The effects of Vc on melanoma cell proliferation, cell migration, and apoptosis are assessed by the CCK-8 assay, wound healing assay, Transwell assay, and flow cytometry. The effect of Vc on tumor growth *in vivo* is determined using an xenograft mouse model. Molecular and biochemical methods are used to elucidate the mechanisms by which Vc modulates melanoma progression. We find that low-dose Vc promotes melanoma cell chemotactic migration and xenograft tumor growth, whereas high-dose Vc inhibits cell proliferation and migration, induces apoptosis, and suppresses tumor growth. Mechanistically, we identify a novel axis involving extracellular signal-regulated kinase (ERK), protein tyrosine phosphatase nonreceptor type 12 (PTPN12), and Janus kinase 2 (JAK2). Specifically, low-dose Vc-induced ERK activation increases PTPN12 phosphorylation at Ser^{434}, which inhibits PTPN12-mediated dephosphorylation of JAK2, thereby increasing JAK2 activity. In contrast, high-dose Vc exerts the opposite effect by suppressing this axis. Furthermore, Vc regulates melanoma cell migration in a PTPN12-dependent manner. Our findings elucidate a novel mechanism involving the ERK-PTPN12-JAK2 axis in the influence of Vc on melanoma progression, underscore the therapeutic potential of high-dose Vc as a promising adjunctive therapy, and highlight the potential risk of low-dose supplementation.

Key words ERK, JAK2, oncotherapy, PTPN12, vitamin C

Introduction

Vitamin C (Vc, also known as ascorbic acid or ascorbate) is an essential nutrient that functions as a potent antioxidant and a critical cofactor for numerous dioxygenases [1]. The therapeutic potential of Vc in oncology has been debated since Linus Pauling first proposed its antitumor effects in the 1970s [2]. However, subsequent clinical trials failed to demonstrate significant therapeutic benefits of orally administered Vc in cancer patients [3,4]. The route of administration was later established as a decisive factor influencing the efficacy of high-dose Vc therapy [5]. More recently, high-dose Vc selectively kills KRAS- and BRAF-mutant colorectal cancer cells by targeting GAPDH [6] and induces pyroptosis in LKB1-deficient lung cancer cells [7]. Nevertheless, the precise mechanisms through which high-dose Vc exerts its anticancer effects remain controversial [8]. Paradoxically, accumulating evidence suggests that antioxidants, including Vc, may promote tumorigenesis under certain conditions [9]. This phenomenon is exemplified in melanoma, where low concentrations of Vc promote tumor growth, whereas high concentrations of Vc induce cytotoxicity [10]. This concentration-dependent duality underscores the

© The Author(s) 2026. This is an open access article distributed under the terms of the Creative Commons Attribution License (https://creativecommons.org/licenses/by/4.0/).

imperative to further elucidate the underlying mechanisms.

The Janus kinase-signal transducer and activator of transcription (JAK-STAT) pathway is a key oncogenic signaling cascade that is frequently hyperactivated in cancer [11,12]. A central component of this pathway, Janus kinase 2 (JAK2), regulates cell survival by controlling the expression of the antiapoptotic protein Bcl-XL [13]. Mechanistically, JAK2 activity is negatively regulated by protein tyrosine phosphatases (PTPs), which dephosphorylate key residues on JAK kinases via direct binding [14,15]. We previously demonstrated that sodium-dependent Vc transporter 2 (SVCT2) functions as a receptor-like transporter to mediate JAK2 activation induced by 50 μg/mL Vc [16]. However, the regulatory effects of high-dose Vc on JAK2 activity remain unknown. Here, we hypothesized that a specific PTP mediates this concentration-dependent regulation of JAK2 in response to Vc.

Protein tyrosine phosphatase nonreceptor type 12 (PTPN12) is a tumor suppressor that inhibits tumor cell proliferation and migration while simultaneously promoting apoptosis [17,18]. Its phosphatase activity is modulated by phosphorylation at specific residues, including Ser^{19}, Ser^{39}, and Ser^{434} [19–21]. Notably, PTPN12 is a known substrate of extracellular signal-regulated kinase 1/2 (ERK1/2) [22], a central kinase in the mitogen-activated protein kinase (MAPK) pathway. The MAPK/ERK pathway is hyperactivated in more than 85% of cancers and drives cancer cell proliferation [23,24]. Intriguingly, Vc-induced low-dose activation and high-dose inhibition of ERK1/2 activity occur in a concentration-dependent manner [25,26]. However, the regulatory interplay between Vc and PTPN12 and the potential role of PTPN12 in modulating JAK2 activity remain to be characterized.

In this study, we revealed the dual concentration-dependent effects of Vc on melanoma progression mediated by the ERK-PTPN12-JAK2 axis. Low-dose Vc promotes tumor progression by activating the ERK-PTPN12-JAK2 axis, whereas high-dose Vc suppresses tumor growth by inhibiting this axis. Moreover, Vc regulates melanoma cell migration in a PTPN12-dependent manner. Collectively, these findings reveal a novel molecular mechanism underlying the opposing effects of Vc on melanoma, highlighting its potential role as an adjuvant in cancer therapy, which requires further preclinical validation.

Materials and Methods

Cell culture

All cell lines were obtained from the Cell Bank of the Chinese Academy of Sciences (Shanghai, China). The cells were cultured in Dulbecco's modified Eagle's medium (DMEM; Thermo Fisher Scientific, Waltham, USA) supplemented with 10% fetal bovine serum (FBS; Biological Industries, Beit HaEmek, Israel) at 37°C in a humidified incubator containing 5% CO_2 [27]. All the cell lines were confirmed to be free of mycoplasma contamination.

Plasmid construction

Jak2 (NCBI Gene ID: 16452) with a Clover tag was provided by Zhuo Han (Northwest A&F University) [16]. The full-length coding sequence of mouse *Ptpn12* (NCBI Gene ID: 19248) was amplified from E14 mouse whole-brain cDNA and subsequently subcloned and inserted into the pEGFP-N1, p3×Flag-CMV10, or pcDNA3-mRuby2 vector (Addgene, Watertown, USA) using the *pEASY*-Basic Seamless Cloning and Assembly Kit (TransGen Biotech, Beijing, China). The full-length coding sequences of mouse *Erk1*, *Erk2*, and *Mek1* (NCBI Gene IDs: 26417, 26413, and 26395) were amplified from E14 mouse whole-brain cDNA and subsequently subcloned and inserted into the p3×Flag-CMV10 vector using the same kit. PTPN12 mutants (C231S, S39A, S420A, S434A, and S434D) were generated by site-directed mutagenesis using splicing by overlap extension PCR. Briefly, two internal mutagenic primers with a 15–20 bp overlapping end were used in separate initial PCRs, each paired with a corresponding external primer, to amplify the upstream and downstream fragments, which were then assembled via overlap extension PCR with the external primers to generate the full-length mutant. All the constructs were verified by Sanger sequencing (Sangon Biotech, Shanghai, China) and aligned against the NCBI database. The sequences of the primers used in this study are presented in Supplementary Table S1.

Transfection, drug treatment and cell lysis

Upon reaching 50%–60% confluence, cells were transfected with the constructed plasmids by using Lipofectamine™ 2000 (Thermo Fisher Scientific) according to the manufacturer's instructions and cultured in Opti-DMEM (Thermo Fisher Scientific) at 37°C for 6 h. The medium was subsequently replaced with fresh culture medium, and the cells were harvested 48 h post transfection. Tg101348 (Tg, a specific inhibitor of JAK2; Selleck, Houston, USA) and PD0325901 (PD, a specific inhibitor of the MEK/ERK pathway; Beyotime, Nantong, China) were prepared as 2 mM stock solutions in dimethyl sulfoxide (DMSO). H 89 2HCl (a specific inhibitor of PKA; Selleck) was prepared as a 30 mM stock solution in DMSO. Cells were pretreated with 2 μM Tg or 2 μM PD for 4 h, or with 30 μM H 89 2HCl for 1 h, before they were treated with Vc (L-ascorbic acid; Sigma-Aldrich, Shanghai, China). Vc was prepared as a 50 mg/mL aqueous stock solution. Final concentrations of 10 μg/mL (low dose) and 500 μg/mL (high dose) were selected on the basis of dose-response studies in B16-F10 melanoma cells, in which 10 μg/mL Vc promoted cell chemotactic migration and 500 μg/mL Vc induced cytotoxicity. For specific mechanistic experiments conducted in HEK293T cells with high plasmid transfection efficiency, such as immunoprecipitation (IP), co-immunoprecipitation (Co-IP), substrate capture, and phosphatase activity assays, 50 μg/mL Vc was used to achieve robust activation of the ERK-PTPN12-JAK2 axis within 20 min (data not shown). After incubation with or without Vc for the indicated time periods, the cells were immediately lysed in cold RIPA buffer (Solarbio, Beijing, China) supplemented with 0.1% protease inhibitor cocktail 1, 1% phosphatase inhibitor cocktail 3, and 0.5% phosphatase inhibitor cocktail 2 (Sigma-Aldrich).

Generation of *Ptpn12*-knockdown cells

To establish a *Ptpn12*-knockdown cell line, the CRISPR/Cas9 system was used in murine melanoma B16-F10 cells. A single guide RNA (sgRNA) targeting the third exon of the mouse *Ptpn12* gene was designed using the CCTop CRISPR/Cas9 online predictor and the CRISPR design tool from the Zhang laboratory website. The sequences of the targeted sgRNAs were as follows: sense, 5′-CACCGTATAATCTGAATCTTGGGA-3′; antisense, 5′-AAACTCC CAAGATTCAGATTATAC-3′. The sequences of the non-targeting control sgRNAs were as follows: sense, 5′-CACCGCGAGG TATTCGGCTCCGCG-3′; antisense, 5′-AAACCGCGGAGCCGAA TACCTCGC-3′. The sgRNAs were annealed and inserted into the pSpCas9(BB)-2A-Puro (PX459) vector (Addgene) linearized with *Bbs*I (Thermo Fisher Scientific). The recombinant plasmids, pCas9-

sgPtpn12 and pCas9-sgControl, were verified by sequencing. B16-F10 cells were transfected with the targeting or control plasmid using Lipofectamine™ 2000. Cells were selected with 1.2 μg/mL puromycin (Abmole, Houston, USA) for 48 h. Surviving cells were cultured in fresh medium for 7–14 days. Individual colonies were picked into 96-well plates using an Olympus SZX16 stereomicroscope (Olympus, Tokyo, Japan) and expanded. When the cells reached approximately 90% confluence, a portion of the cells was lysed with 20 μL of lysis buffer (Sangon Biotech) and subjected to PCR amplification using identification primers for frameshift mutations of *Ptpn12* (forward, 5′-CGCTCTATGGGAAGGCATGA-3′; reverse, 5′-CCAGCACTTGGTAGCTGACA-3′). The PCR products were subsequently cloned and inserted into the T-Vector pMD™19 (Takara, Dalian, China) and sequenced. Clones with *Ptpn12* mutations were identified, and PTPN12 protein expression was confirmed by western blotting.

Cell proliferation assay

Cells were seeded into 96-well plates at 5000 cells/well. After 12 h of incubation, the cells were treated with different doses of Vc for the indicated time periods, as previously described [28]. A CCK-8 assay kit (Beyotime) was subsequently used to assess the effect of Vc on cell proliferation. The culture medium was replaced with 100 μL of fresh medium containing 10% CCK-8 solution and then incubated at 37°C for 2 h. The absorbance at 450 nm was measured using a microplate reader (Thermo Fisher Scientific).

Wound healing assay

Cells were seeded into 48-well plates at 6×10^5 cells/well. When the cells reached 90% confluence, a linear wound was created in the cell monolayer using a 200-μL pipette tip. The cells were treated with 1 μg/mL mitomycin C (Abmole) for 2 h to inhibit proliferation. The medium was then replaced with fresh medium containing different doses of Vc. After 48 h, wound closure was imaged using an ECLIPSE Ti2 inverted microscope (Nikon, Tokyo, Japan). Wound healing rate was calculated using the following formula: Wound healing rate (%) = (Wound $\text{area}_{0\ h}$ − Wound $\text{area}_{48\ h}$)/ Wound $\text{area}_{0\ h} \times 100$ [29].

Transwell assay

A total of 1×10^5 cells suspended in serum-free DMEM were seeded into the upper chamber of a Transwell chamber (NEST, Wuxi, China) equipped with an 8-μm pore-size polycarbonate membrane, and DMEM supplemented with 10% FBS was added to the lower chamber. After migration, the cells remaining on the upper surface of the membrane were removed with a cotton swab. The migrated cells on the lower surface were fixed in 4% (w/v) paraformaldehyde (PFA) for 30 min, permeabilized with methanol for 5 min, and subsequently stained with 0.1% (w/v) crystal violet (Sangon Biotech) at 37°C for 30 min. The membranes were subsequently imaged using the ECLIPSE Ti2 inverted microscope.

Apoptosis assay

Apoptosis was detected using the Dead Cell Apoptosis Kit with Annexin V-Alexa Fluor™ 488 & Propidium Iodide (PI; Thermo Fisher Scientific) following the manufacturer's instructions. Briefly, the cells were resuspended in binding buffer at approximately 2×10^6 cells/mL. The cell suspension was incubated with Annexin V-Alexa Fluor 488 and PI for 15 min. Data were acquired using a BD FACSAria III flow cytometry system (BD Biosciences, Franklin Lakes, USA) and analyzed with FlowJo software (v10.0.7; BD Biosciences).

Xenograft model establishment

All animal protocols were reviewed and approved by the Animal Ethical and Welfare Committee of Northwest A&F University (No. 2021058). Female C57BL/6 mice (5–6 weeks old) were purchased from the Experimental Animal Center of Xi'an Jiaotong University (certificate No. SCXK [SHAAN]-2018-001; Xi'an, China). The mice were housed in isolated ventilated cages (a maximum of 6 mice per cage) at Northwest A&F University and maintained on a 12-h light/dark cycle at 23 ± 2°C and 50% ± 10% humidity, with free access to a standard diet and water. Littermates of the same sex were randomly assigned to experimental groups. To establish xenograft mouse models, 50 μL of sterile normal saline containing 1×10^5 B16-F10 cells was injected subcutaneously into the right flank of each anesthetized mouse. The mice were anesthetized with isoflurane (Sigma-Aldrich; induction: 3%–4%; maintenance: 1%–2%). The tumor dimensions were measured using calipers, and the tumor volume was calculated as $V = 0.5 \times \text{length} \times \text{width}^2$. The mice were euthanized by CO_2 inhalation followed by cervical dislocation.

Intratumoral injection

When the longest tumor diameter reached 5 mm, the tumor-bearing mice were randomly divided into three groups and received intratumoral (i.t.) injections of L-ascorbic acid sodium (Solarbio) every two days, with a fixed injection volume of 50 μL per 0.5 cm^3 tumor volume. The groups were as follows: (1) control group: 29.5 mg/mL NaCl; (2) low-dose (Vc) group: 2.5 mg/mL L-ascorbic acid sodium; and (3) high-dose (Vc) group: 100 mg/mL L-ascorbic acid sodium. In the three groups, the sodium concentration was kept the same to balance the osmotic effect by NaCl supplementation. Mice were sacrificed when the tumor volume exceeded 2000 mm^3, the tumor became ulcerated, or the mice lost more than 20% of their initial body weight.

Western blot analysis

Cells were lysed with cold RIPA buffer supplemented with protease inhibitors and phosphatase inhibitors (Sigma-Aldrich) on ice for 10 min. Cell lysates were separated by 10% SDS-PAGE and then transferred to polyvinylidene difluoride membranes (0.22 μm; Sigma-Aldrich). The membranes were blocked in 5% nonfat milk powder in Tris-buffered saline with 0.1% Tween-20 (TBST) for 2 h, subsequently incubated with primary antibodies overnight at 4°C and then incubated with secondary antibody for 2 h at room temperature. Target proteins were detected using a WesternBright ECL kit (Advansta, San Jose, USA) and imaged with a ChemiDoc™ MP imager (Bio-Rad, Hercules, USA). The antibodies used were anti-Flag (1:3000, F1804; Sigma-Aldrich), anti-GFP (1:1000, 66002-1-Ig; Proteintech, Wuhan, China), anti-JAK2 (1:250, sc-390539; Santa Cruz, Dallas, USA), anti-pJAK2 (1:500, 3771; CST, Danvers, USA), anti-ERK1/2 (1:3000, 4695; CST), anti-pERK1/2 (1:5000, 9101; CST), anti-PTPN12 (1:500, sc-271351; Santa Cruz), anti-GAPDH (1:3000, HC301; TransGen), anti-β-Tubulin (1:3000, HC101; TransGen), anti-phosphotyrosine (1:800, 9411; CST), anti-phosphoserine (1:250, sc-81514; Santa Cruz), HRP-labeled goat anti-rabbit IgG(H+L) (1:3000, A0208; Beyotime), and HRP-labeled goat anti-mouse IgG(H+L) (1:3000, A0216; Beyotime).

IP and Co-IP assays

Cells were lysed in IP lysis buffer (25 mM Tris-HCl, pH 7.4, 150 mM NaCl, 1% NP-40, 1 mM EDTA, and 5% glycerol) supplemented with 0.1% protease inhibitor cocktail, 0.5% phosphatase inhibitor cocktail 3, and 0.2% phosphatase inhibitor cocktail 2 (Sigma-Aldrich). The lysates were subsequently centrifuged at 15,000 *g* for 10 min at 4°C. The supernatants were incubated with anti-Flag antibody (1:100, F1804; Sigma-Aldrich) or control immunoglobulin G (IgG; 1:100, A7028; Beyotime) at 4°C for 6 h. The precipitated proteins were captured with Pierce Protein A/G Agarose (Thermo Fisher Scientific) at 4°C for 2 h. After three washes in IP lysis buffer, the bound proteins were eluted in 5× SDS loading buffer (Beyotime) and analyzed by western blotting. The methods used were the same as those described in our earlier papers [30].

Immunofluorescence assay

Cells cultured on glass coverslips were subsequently fixed with 4% (w/v) paraformaldehyde (PFA) for 15 min and permeabilized with 0.2% Triton X-100 for 20 min. After blocking with 1% FBS for 1 h, the cells were incubated with anti-Flag antibody (1:500; F1804; Sigma-Aldrich) at 4°C overnight, followed by incubation with Alexa Fluor 488-conjugated secondary antibodies (1:500; A-11029) or Alexa Fluor 555-conjugated secondary antibodies (1:500; A-21424) from Thermo Fisher Scientific for 2 h. Coverslips were mounted with Antifade Mounting Medium (Beyotime) and imaged using a FLUOVIEW FV3000 confocal microscope (Olympus).

Förster resonance energy transfer

Förster resonance energy transfer (FRET) efficiency between proteins was measured using sensitized emission FRET, with mRuby2 as the donor and Clover as the acceptor [31]. HEK293T cells were cotransfected with pcDNA3-mRuby2-Ptpn12 and pcDNA3-Clover-Jak2 for 36 h and then seeded into 35-mm glass-bottom dishes (NEST) at the desired density. When the cells reached 60%–80% confluence, they were imaged using a FLUOVIEW FV3000 confocal microscope, and sensitized emission FRET analysis was performed with cellSens Dimension (v3.1; Olympus).

For the acquisition of fluorescence images for FRET, three imaging channels with distinct excitation/emission combinations were used. FRET channel: excitation at 488 nm (donor), emission collected at 560–630 nm (acceptor); Donor channel: excitation at 488 nm, emission at 510–550 nm; Acceptor channel: excitation at 561 nm, emission at 560–630 nm. The sequential scan option was set to "None". For FRET correction, two images (FRET and donor channels) were acquired from a donor-only sample, and two images (FRET and acceptor channels) were acquired from an acceptor-only sample. The parameters for the FRET correction images were the same as those for the acquisition of the FRET images.

The appropriate reference images were loaded into cellSens Dimension, and FRET correction was performed using the *FRET correction* dialog box. After the appropriate reference images, background regions, and at least five regions of interest (ROIs) were selected, FRET correction was performed, and the correction factors DSBT a (FRET channel/donor channel) and ASBT b (FRET channel/acceptor channel) were recorded. Each correction factor was averaged from three replicates.

FRET images were loaded into cellSens Dimension, and FRET analysis was performed using the FRET analysis dialog box. Afterward, the appropriate channels were selected, and an ROI was defined as the background. The "Xia" computation method (described in [32]) was chosen from the method list. After loading the correction factors, FRET analysis was executed. In accordance with the manual, the FRET map resulting from the Xia method is a gray-value image that automatically has a predefined pseudocolor table. High values are displayed in red with this pseudocolor look-up table, and low ratio values are displayed in magenta.

Silver staining assay

The proteins were separated by 10% SDS-PAGE and visualized using a PAGE Gel Silver Staining kit (Solarbio). The gel was sequentially incubated in fixation buffer and sensitizing solution for 30 min each, washed three times with deionized water, incubated in silver staining solution for 40 min, and then developed and terminated with stop buffer. The stained gel was imaged using the ChemiDoc™ MP imager.

Phosphoproteome analysis

Quantitative phosphoproteomic analysis of Vc-stimulated F9 cells was performed using multiplex tandem mass tag (TMT) labeling coupled with liquid chromatography-mass spectrometry (LC-MS). Briefly, F9 cells were treated with 50 μg/mL Vc for 20 min and then lysed in lysis buffer containing 100 mM NH_4HCO_3, pH 8.0, 6 M urea, 0.2% SDS, and 1% phosphatase inhibitor cocktail 3. The lysates were immediately frozen in liquid nitrogen. Phosphoproteomic analysis was carried out by Novogene (Beijing, China). The raw data were searched against the *Mus musculus* UniProt database (release 2019.01.18; 85,165 sequences) using Proteome Discoverer 2.2 (Thermo Fisher Scientific).

Phosphatase assay

HEK293T cells were transfected with Flag-tagged PTPN12 and PTPN12 mutants. Cells were lysed in IP lysis buffer supplemented with 1 mM PMSF (Solarbio), and proteins were immunoprecipitated using an anti-Flag antibody (Sigma-Aldrich). Immunoprecipitates were assayed for phosphatase activity as described previously [33]. Briefly, the immunoprecipitates were incubated with pNPP (5 mM final concentration) in phosphatase assay buffer at 37°C for 1 h, and the reaction was stopped by the addition of 1 M NaOH. The absorbance at 405 nm was measured using a microplate reader (Thermo Fisher Scientific).

Statistical analysis

GraphPad Prism (v9.0; GraphPad Software, La Jolla, USA) was used for data analysis. Data are presented as the mean ± SD from at least three independent replicates. Statistical significance was determined by two-tailed Student's *t* test for two-group comparisons and by one-way ANOVA with Dunnett's post hoc test or two-way ANOVA with Tukey's *post hoc* test for multiple comparisons. $P < 0.05$ was considered to indicate statistical significance.

Results

Vc exerts a concentration-dependent dual effect on melanoma progression

To assess the effects of different doses of Vc on melanoma progression, we first performed a CCK-8 assay to evaluate the effects of low-dose (10 μg/mL) and high-dose (500 μg/mL) Vc on the proliferation of the murine melanoma cell line B16-F10. As shown in Figure 1A, high-dose Vc treatment significantly inhibited B16-F10

cell proliferation, but low-dose Vc treatment did not significantly affect this process. Next, we examined cell migration using wound healing and Transwell assays. Low-dose Vc enhanced chemotactic migration in the Transwell assay but did not significantly promote wound-closure migration. In contrast, high-dose Vc potently inhibited both processes (Figure 1B,C). As shown in Figure 1D, high-dose Vc markedly induced apoptosis in B16-F10 cells, whereas the change in apoptosis induced by low-dose Vc did not reach statistical significance. We further constructed xenograft tumor models using B16-F10 cells, and intratumoral injection of low- or high-dose Vc was performed. The growth of xenograft tumors was promoted by low-dose Vc but retarded by high-dose Vc (Figure 1E). Notably, previous studies have demonstrated that Vc concentrations exceeding 500 μg/mL are readily achievable in human plasma without significant toxicity [5,34,35], and as our results showed here, 500 μg/mL Vc was sufficient to kill melanoma cells. Collectively, these observations suggest that high-dose Vc may represent a promising adjunctive therapy for melanoma, whereas low-dose Vc has the potential to promote melanoma progression. However, further preclinical validation is needed.

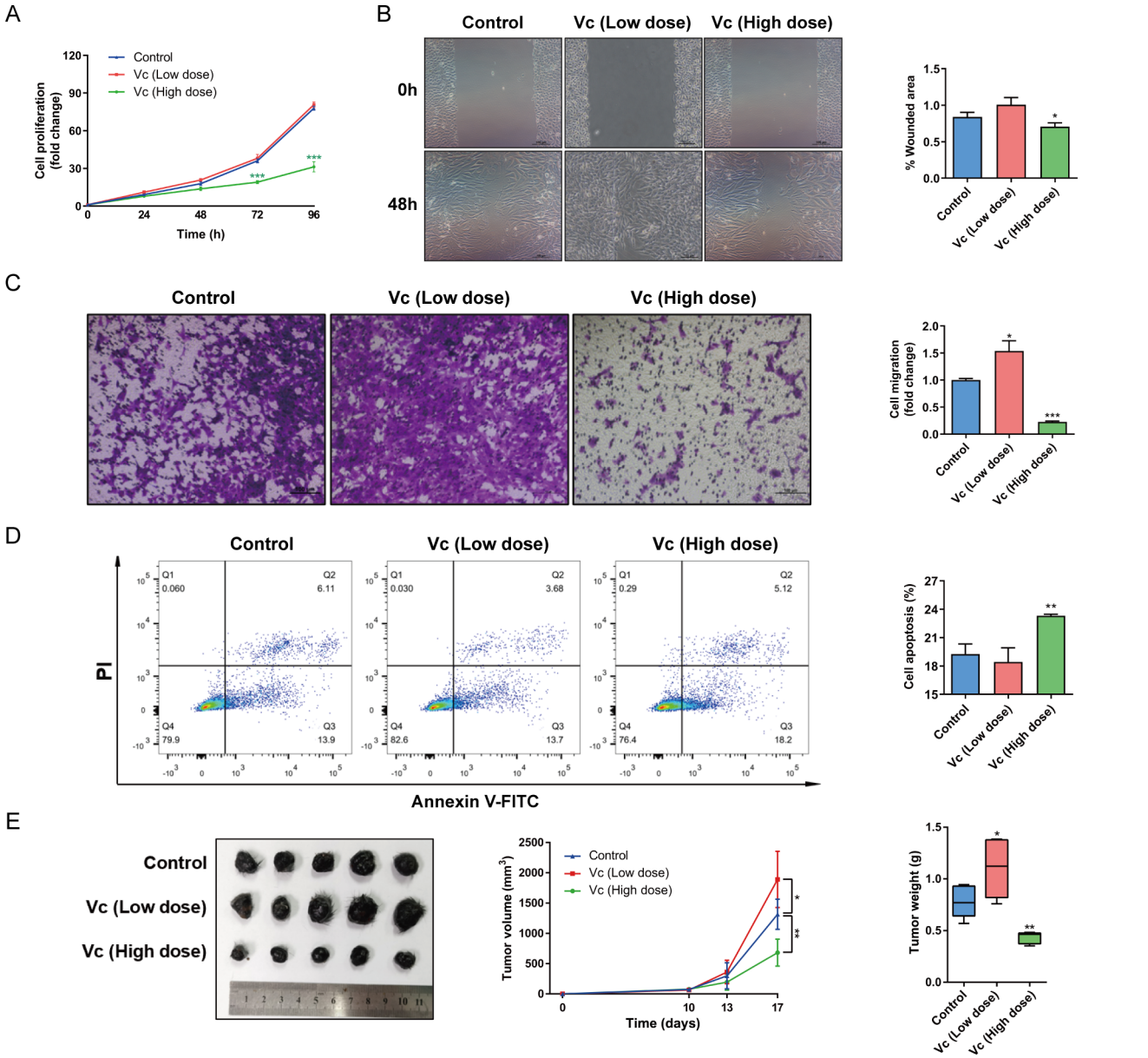


Figure 1. Vc plays a concentration-dependent dual role in melanoma progression (A) The proliferation of B16-F10 cells treated with different doses of Vc was determined by a CCK8 assay. (B,C) The migration ability of B16-F10 cells treated with different doses of Vc was assessed by a wound healing assay (B) and a Transwell assay (C). Scale bar, 100 μm. (D) The apoptosis of B16-F10 cells treated with different doses of Vc was detected by flow cytometry. (E) Effects of different doses of Vc on xenograft tumor growth *in vivo*. Left: representative images of tumors from B16-F10 mice (n = 5) after intratumoral injection of Vc. Right: the tumor growth curve was plotted using xenograft tumor volume data, and tumor weight was measured after tumor excision. In (A–D), the low-dose Vc concentration was 10 μg/mL, and the high-dose Vc concentration was 500 μg/mL. Data are presented as the mean ± SD. Two-tailed Student's t test compared with the control. $^{*}P < 0.05$, $^{**}P < 0.01$, $^{***}P < 0.001$.

Vc exerts a concentration-dependent dual effect on melanoma progression, which involves the regulation of JAK2 activity

Our previous study revealed that SVCT2 functions as a receptor-like transporter to mediate 50 μg/mL Vc-induced JAK2 activation [16]. To determine whether the Vc-induced regulation of JAK2 activity is correlated with melanoma progression, we assessed JAK2 phosphorylation levels in B16-F10 cells following Vc treatment. Interestingly, low-dose Vc treatment increased JAK2 phosphorylation, whereas high-dose Vc treatment significantly inhibited this activity (Figure 2A).

Given the prevalence of JAK2 hyperactivation in cancer, we hypothesize that high-dose Vc impedes melanoma progression by negatively regulating JAK2 activity. To validate this hypothesis, we treated B16-F10 cells with either Tg alone or in combination with Vc and assessed cell proliferation, migration, and apoptosis. As expected, Tg alone significantly inhibited proliferation and migration and promoted apoptosis, which is consistent with the established oncogenic role of JAK2 signaling. Compared with Tg alone, the combination of high-dose Vc and Tg resulted in even more pronounced suppression of cell proliferation and greater induction of apoptosis, suggesting that JAK2 inhibition contributes to the cytotoxic effect of high-dose Vc and that additional antitumor mechanisms may also be involved (Figure 2B–E). Accordingly, Tg treatment significantly suppressed low-dose Vc-induced chemotactic migration (Figure 2D), supporting a role for JAK2 phosphorylation in the tumor-promoting effect of low-dose Vc. Additionally, Tg significantly increased high-dose Vc-induced apoptosis. Collectively, these findings demonstrate that pharmacological inhibition of JAK2 abrogates the tumor-promoting effect of low-dose Vc and enhances the antitumor effect of high-dose Vc, confirming the involvement of JAK2 activity in the biphasic effects of Vc on melanoma.

PTPN12 contributes to the Vc-induced regulation of JAK2 activity

It has been reported that the binding of PTPs to JAK2 mediates JAK2 dephosphorylation and inhibits its activity [14,36]. We therefore hypothesized that JAK2 may serve as a substrate for PTPN12, with its activity modulated by PTPN12. To investigate the role of PTPN12 in the Vc-induced regulation of JAK2 activity, we performed a quantitative phosphoproteomic analysis of the Vc-stimulated F9 cells. The data revealed that the phosphorylation of PTPN12 at Ser^{434} was significantly upregulated following 50 μg/mL Vc treatment (Supplementary Figure S1A). Next, the serine phosphorylation (pSer) of PTPN12 was validated with Vc stimulation over time. As shown in Figure 3A, the pSer levels of PTPN12 peaked at 20 min after 50 μg/mL Vc supplementation but then decreased after 30 min. We next evaluated the pSer levels of PTPN12 in B16-F10 cells treated with low- and high-dose Vc. Consistent with the changes in JAK2 activity, low-dose Vc increased the pSer level of PTPN12, whereas high-dose Vc significantly decreased it (Figure 3B). Similar results were obtained in HEK293T and HeLa cells (Supplementary Figure S1B). Thus, Vc-modulated JAK2 phosphorylation is correlated with changes in PTPN12 activity. To test whether PTPN12 functions as an upstream mediator of JAK2, *Ptpn12* was knocked down using the CRISPR/Cas9 system in the murine melanoma cell line B16-F10 (Supplementary Figure S1C,D). Compared with those in wild-type B16-F10 cells, pJAK2 levels in *Ptpn12*-knockdown cells were greater (Figure 3C), indicating that PTPN12 contributes to JAK2 dephosphorylation. The response of JAK2 phosphorylation to Vc in *Ptpn12*-knockdown cells was subsequently analyzed. In contrast to that in wild-type B16-F10 cells, the change in JAK2 phosphorylation in *Ptpn12*-knockdown cells was not statistically significant (Figure 3D,E). These data demonstrate that PTPN12 activity contributes to the Vc-mediated modulation of JAK2 phosphorylation.

To further determine whether JAK2 is a substrate of PTPN12, we first examined the subcellular localization of JAK2 and PTPN12 in HEK293T cells. As expected, JAK2 colocalized with PTPN12 in the cytoplasm and membrane (Figure 3F). Sensitized emission FRET and Co-IP assays confirmed that JAK2 interacts with PTPN12 in HEK293T cells (Figure 3G,H). Moreover, as shown in Figure 3H, JAK2 phosphorylation was significantly lower in cells coexpressing wild-type PTPN12 than in cells without exogenous PTPN12, whereas pJAK2 levels were significantly greater in cells coexpressing the catalytically inactive PTPN12 C231S mutant. These results suggested that JAK2 is a substrate of PTPN12, which is consistent with the observation that pJAK2 levels were consistently higher in *Ptpn12*-knockdown cells than in wild-type B16-F10 cells. A substrate trapping assay further validated these findings: the amount of JAK2 coprecipitated with wild-type PTPN12 was significantly lower than that coprecipitated with the PTPN12 C231S mutant. To verify whether PTPN12 phosphorylation induced by 50 μg/mL Vc is associated with JAK2 activation, wild-type PTPN12 was coexpressed with JAK2 in HEK293T cells with or without 50 μg/mL Vc. Treatment with 50 μg/mL Vc enhanced the coimmunoprecipitation of JAK2 with PTPN12 (Figure 3I). Accordingly, PTPN12 significantly promoted JAK2 dephosphorylation in the absence of 50 μg/mL Vc, whereas JAK2 phosphorylation markedly increased in the presence of 50 μg/mL Vc (Figure 3I). In conclusion, JAK2 is a substrate of PTPN12, and its interaction is regulated by Vc. Furthermore, Vc modulates JAK2 activity by influencing PTPN12 phosphorylation.

Vc regulates the phosphatase activity of PTPN12 through ERK-mediated phosphorylation at Ser^{434}

Previous studies have shown that Vc modulates the MAPK/ERK and JAK/STAT pathways [16,26,37] and that PTPN12 is a substrate of ERK1/2 [22]. To determine whether ERK mediates 50 μg/mL Vc-induced PTPN12 phosphorylation, we evaluated PTPN12 and JAK2 phosphorylation following PD treatment. Treatment with 50 μg/mL Vc increased the pSer level of PTPN12, whereas PD reduced this effect (Figure 4A). PD also significantly blocked JAK2 phosphorylation induced by 50 μg/mL Vc (Figure 4B), suggesting that ERK acts upstream of PTPN12 and is involved in JAK2 activation. Next, we assessed ERK phosphorylation following Vc treatment. In B16-F10 cells, low-dose Vc treatment induced ERK activation within 24 h, whereas high-dose Vc treatment suppressed ERK activation (Figure 4C), mirroring the changes in PTPN12 and JAK2 activity. In *Ptpn12*-knockdown cells, ERK phosphorylation responded similarly to that in wild-type cells (Figure 4D,E). However, the change in JAK2 activation in *Ptpn12*-knockdown cells did not significantly differ from that in control cells upon Vc treatment (Figure 3D,E), which is consistent with a model in which PTPN12 acts downstream of ERK and upstream of JAK2. These results suggest that Vc-induced ERK activity mediates the serine phosphorylation of PTPN12.

To validate whether the phosphorylation of PTPN12 at Ser^{434} is

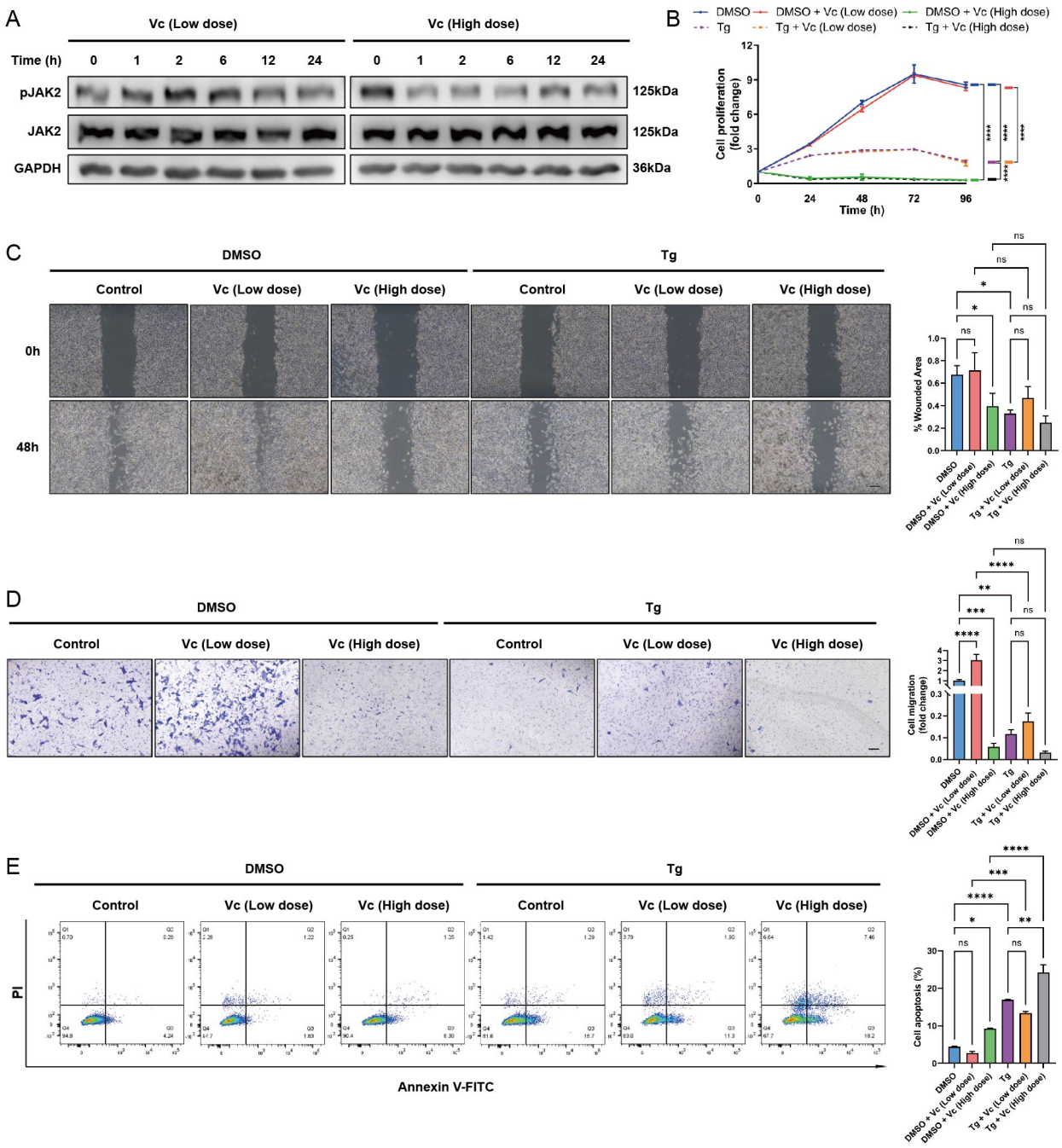


Figure 2. Vc plays a concentration-dependent dual role in melanoma progression, which involves the regulation of JAK2 activity (A) B16-F10 cells were treated with a low dose (10 μg/mL) or a high dose (500 μg/mL) of Vc and lysed at the indicated time periods. The lysates were immunoblotted as indicated. (B) The proliferation of B16-F10 cells treated with different doses of Vc alone, Tg101348 (Tg) alone, or Tg in combination with Vc was determined by a CCK8 assay. (C,D) The migration ability of B16-F10 cells treated with different doses of Vc alone, Tg alone, or Tg in combination with Vc was detected by a wound healing assay (C) and a Transwell assay (D). Scale bar, 100 μm. (E) Apoptosis of B16-F10 cells treated with different doses of Vc alone, Tg alone, or Tg in combination with Vc was detected by flow cytometry. The low-dose Vc concentration was 10 μg/mL, and the high-dose Vc concentration was 500 μg/mL. The data are presented as the mean ± SD. Statistical significance was determined by two-way ANOVA followed by Tukey's multiple comparisons test. $*P<0.05$, $**P<0.01$, $***P<0.001$, $****P<0.0001$. ns, not significant.

responsive to 50 μg/mL Vc-induced ERK activation, we constructed a PTPN12 S434A mutant, along with two control mutants: PTPN12 S39A (both Ser^{39} and Ser^{434} of PTPN12 can be phosphorylated by PKA in previous reports) [38] and PTPN12 S420A (Ser^{420} is a predicted ERK phosphorylation site). Immunofluorescence assay confirmed that mutations at Ser^{39}, Ser^{420} and Ser^{434} in PTPN12 did not alter the subcellular localization of PTPN12 (Supplementary Figure S2A). IP showed that 50 μg/mL Vc increased the pSer levels

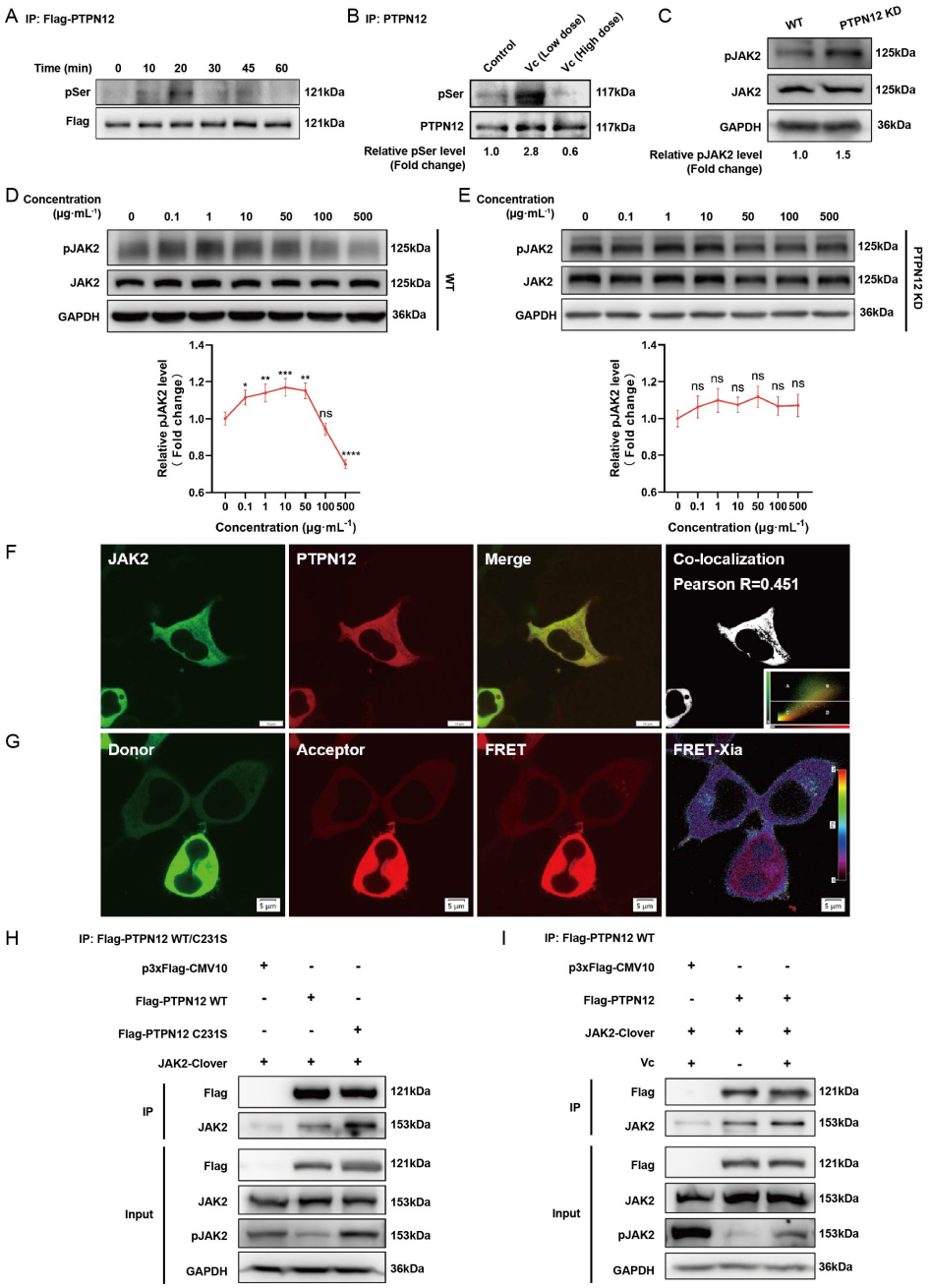


Figure 3. PTPN12 participates in the Vc-induced regulation of JAK2 activity (A) HEK293T cells were transfected with Flag-tagged PTPN12 for 36 h and then treated with 50 μg/mL Vc for the indicated time periods. Flag-tagged PTPN12 was immunoprecipitated, and the precipitates were blotted for phosphoserine. pSer, phospho-serine. (B) B16-F10 cells were treated with low doses (10 μg/mL) or high doses (500 μg/mL) of Vc and lysed at the indicated time periods. PTPN12 was immunoprecipitated, and the precipitates were blotted for phosphoserine. pSer, phospho-serine. (C) Wild-type B16-F10 cells (WT) and *Ptpn12*-knockdown B16-F10 cells were lysed and immunoblotted for endogenous pJAK2, total JAK2 and GAPDH expression. The knockdown efficiency was verified (data shown in Supplementary Figure S1C,D). (D,E) Wild-type and *Ptpn12*-knockdown B16-F10 cells were treated with Vc at the indicated concentrations (0–500 μg/mL) for 20 min. Lysates were immunoblotted as indicated. (F) Colocalization of Flag-PTPN12 and JAK2-Clover in HEK293T cells. The illustration on the lower right shows a scatterplot in which the pixels were located more or less along a diagonal line. All of the pixels whose intensities were in the B quadrant are shown in white. Scale bar, 10 μm. (G) Representative confocal images of JAK2-Clover (donor), PTPN12-mRuby2 (acceptor), FRET and FRET maps. HEK293T cells were cotransfected with JAK2-Clover and PTPN12-mRuby2 for 36 h, after which the cells were photographed using a confocal microscope for FRET analysis. The FRET map resulting from the Xia method is displayed as a pseudocolor table. High values are displayed in red, and low ratio values are displayed in magenta. Scale bar, 5 μm. (H,I) HEK293T cells were cotransfected with Flag-tagged PTPN12 WT/PTPN12 C231S and JAK2-Clover as indicated for 36 h, after which the cells were lysed, and Flag-PTPN12 was immunoprecipitated. The precipitates and input were blotted as indicated. In (I), cells were treated with 50 μg/mL Vc for 20 min. Data are presented as the mean ± SD. Statistical significance was determined by one-way ANOVA followed by Dunnett's multiple comparisons test. $^{*}P < 0.05$, $^{**}P < 0.01$, $^{**}P < 0.001$, $^{****}P < 0.0001$. ns, not significant.

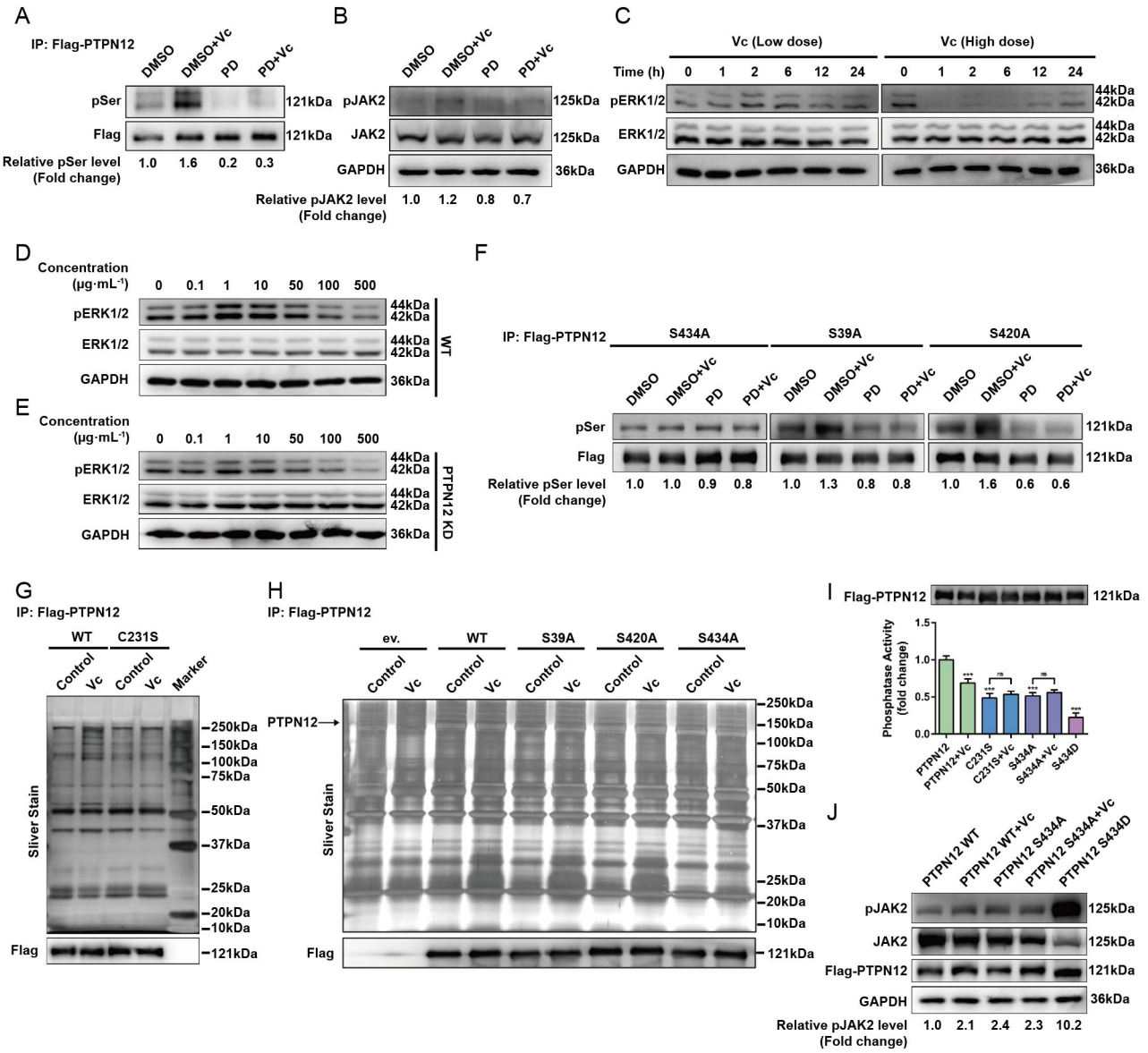


Figure 4. Dependence of PTPN12-mediated JAK2 dephosphorylation on Vc-induced ERK activity (A) HEK293T cells were transfected with Flag-tagged PTPN12 as indicated for 36 h, and the cells were pretreated with PD0325901 (PD, 2 μM) or dimethyl sulfoxide (DMSO) for 4 h. Then, the cells were treated with 50 μg/mL Vc for 20 min and lysed immediately. Flag-tagged PTPN12 was immunoprecipitated, and the precipitates were blotted for phosphoserine. (B) F9 cells were pretreated with PD (2 μM) or DMSO for 4 h and then treated with 50 μg/mL Vc for 30 min. Lysates were immunoblotted as indicated. The effect of PD was validated, as shown in Supplementary Figure S2D. (C) B16-F10 cells were treated with low dose (10 μg/mL) or high dose (500 μg/mL) of Vc and lysed at the indicated time periods. The lysates were immunoblotted as indicated. (D,E) Wild-type and *Ptpn12*-knockdown B16-F10 cells were treated with Vc at the indicated concentrations (0–500 μg/mL) for 20 min. Lysates were immunoblotted as indicated. (F) HEK293T cells were transfected with Flag-tagged PTPN12 mutants as indicated for 36 h and pretreated with PD (2 μM) or DMSO for 4 h. Then, the cells were treated with 50 μg/mL Vc for 20 min and lysed immediately. Flag-tagged PTPN12 mutants were immunoprecipitated, and the precipitates were blotted for phosphoserine. (G) HEK293T cells were transfected with Flag-tagged wild-type (WT) PTPN12 or PTPN12 C231S for 36 h, treated with 50 μg/mL Vc for 20 min and lysed immediately. Flag-tagged PTPN12 was immunoprecipitated, and the precipitates were analyzed by silver staining. (H) HEK293T cells were transfected with Flag-tagged wild-type PTPN12, PTPN12 mutants or empty vector (ev.). As indicated, after 36 h, the cells were treated with 50 μg/mL Vc for 20 min and lysed immediately. Flag-tagged PTPN12 was immunoprecipitated, and the precipitates were analyzed by silver staining. (I) Evaluation of the phosphatase activity of PTPN12 and PTPN12 mutants. HEK293T cells were transfected with Flag-tagged wild-type PTPN12 or PTPN12 mutants for 36 h and then treated with 50 μg/mL Vc for 20 min. Flag-tagged PTPN12 was immunoprecipitated, and the precipitates were analyzed using pNPP as a substrate for phosphatase activity or blotted for a Flag tag. The error bars represent the SDs of five replicates. Two-tailed Student's *t* test was applied. ***$P < 0.001$. ns, not significant. (J) HEK293T cells were cotransfected with Flag-tagged wild-type PTPN12/PTPN12 mutants and JAK2 Clover as indicated for 36 h, after which the cells were treated with 50 μg/mL Vc for 20 min and lysed immediately. The lysates were immunoblotted as indicated.

of PTPN12 S39A and PTPN12 S420A, and these effects were significantly blocked by PD. In contrast, the pSer level of PTPN12 S434A did not significantly change in response to 50 μg/mL Vc or PD (Figure 4F), indicating that Ser^{434} is the primary ERK-targeted phosphorylation site on PTPN12 in response to 50 μg/mL Vc. Furthermore, H 89 2HCl did not significantly reduce basal or 50 μg/mL Vc-induced PTPN12 phosphorylation (Supplementary Figure S2B), suggesting that PKA may not play a major role in this process.

PTPN12 is a nonreceptor protein tyrosine phosphatase (PTP) family member with a deep pocket for phosphotyrosine recognition [39]. Catalytically inactive PTP mutants do not possess catalytic activity but appear to bind tightly to tyrosine-phosphorylated substrates [40]. We therefore used a substrate-trapping approach to test the effect of 50 μg/mL Vc on the activity of PTPN12. Wild-type PTPN12 and PTPN12 C231S were immunoprecipitated from HEK293T cell lysates, and the precipitates were analyzed by silver staining. More proteins pulled down by wild-type PTPN12 in response to 50 μg/mL Vc treatment, whereas PTPN12 C231S did not significantly change in response to 50 μg/mL Vc stimulation (Figure 4G). Additionally, the levels of tyrosine phosphorylation (pTyr) in the precipitates were detected. As shown in Supplementary Figure S2C, 50 μg/mL Vc treatment increased the pTyr levels of proteins that coprecipitated with wild-type PTPN12. In contrast, proteins coprecipitated with the inactive PTPN12 C231S mutant presented higher basal pTyr levels, which did not significantly change upon Vc treatment. These results suggest that 50 μg/mL Vc may induce PTPN12 inactivation.

In addition, the levels of proteins that coprecipitated with wild-type PTPN12, as well as with the S39A and S420A mutants, were more enriched in cells treated with 50 μg/mL Vc than in untreated cells. In contrast, PTPN12 S434A displayed lower substrate affinity, and the change in the levels of coprecipitated proteins upon 50 μg/mL Vc stimulation did not reach statistical significance (Figure 4H), suggesting that the phosphorylation of PTPN12 at Ser^{434} leads to the inactivation of PTPN12. To further confirm the above results, PTPN12 S434D, a phosphorylation-mimicking mutant, was constructed. We then performed phosphatase assays *in vitro* using pNPP (p-nitrophenyl phosphate) as a phosphatase substrate. As shown in Figure 4I, wild-type PTPN12 activity was significantly lower (25%) in cells treated with 50 μg/mL Vc than in cells not treated with Vc. The PTPN12 C231S mutant exhibited a reduction in phosphatase activity, but the change in response to 50 μg/mL Vc stimulation was not statistically significant. Although different from the results of the substrate trapping assay, PTPN12 S434A exhibited an unexpected decrease in phosphatase activity, which may be because pNPP is a small chemical molecule rather than a protein substrate. However, the phosphatase activity of PTPN12 S434A did not significantly change upon treatment with 50 μg/mL Vc, whereas the phosphatase activity of PTPN12 S434D was even lower. These findings indicate that 50 μg/mL Vc-induced phosphorylation of PTPN12 at Ser^{434} inhibits its phosphatase activity. We then evaluated JAK2 phosphorylation in cells coexpressing JAK2 with wild-type PTPN12 or its mutants. As shown in Figure 4J, 50 μg/mL Vc significantly increased pJAK2 levels in the presence of wild-type PTPN12. In contrast, pJAK2 levels did not significantly change upon treatment with 50 μg/mL Vc in cells expressing the S434A mutant. Moreover, the low-phosphatase-activity mutant PTPN12 S434D led to a dramatic increase in JAK2 phosphorylation. These results demonstrate that PTPN12-mediated dephosphorylation of JAK2 depends on ERK-dependent phosphorylation of PTPN12 at Ser^{434}.

Taken together, our findings indicate that Vc influences melanoma progression through the ERK-PTPN12-JAK2 axis, further revealing the molecular mechanism underlying its dual concentration-dependent effects.

Ptpn12 knockdown abrogates Vc-induced migration in melanoma cells

PTPN12 is abnormally expressed in malignant melanoma [41] and is closely associated with tumor cell proliferation and migration [20,42,43]. To elucidate the role of the tumor suppressor PTPN12 in melanoma progression, the phenotype of *Ptpn12*-knockdown cells was examined. Our results revealed that knockdown of *Ptpn12* promoted the proliferation and migration but inhibited the apoptosis of B16-F10 cells (Figure 5A–D). Then, xenograft tumor models using wild-type or *Ptpn12*-knockdown B16-F10 cells were constructed. As expected, knockdown of *Ptpn12* promoted the growth of xenograft tumors (Figure 5E).

On the basis of the finding that the activity of PTPN12 is regulated by Vc, we hypothesized that PTPN12 plays a crucial role in Vc-mediated tumor therapy. To validate this hypothesis, the phenotype of the *Ptpn12*-knockdown cells was detected under low- and high-dose Vc treatment. Intriguingly, the migration ability of the *Ptpn12*-knockdown cells did not significantly change with Vc treatment, regardless of the dose (Figure 5F–H). In contrast, high-dose Vc treatment significantly inhibited the proliferation and promoted the apoptosis of *Ptpn12*-knockdown cells (Supplementary Figure S3A, B), similar to our observations in wild-type B16-F10 cells (Figure 1A–D); however, low-dose Vc treatment did not significantly affect either process. These findings suggest that PTPN12 specifically affects tumor migration, which is consistent with previous reports that PTPN12 inhibits tumor migration [44]. Collectively, the results of this study demonstrate that the concentration of Vc influences melanoma progression, at least in part, through the ERK-PTPN12-JAK2 axis and that its effect on cell migration is PTPN12-dependent.

Discussion

In this study, we provided evidence that Vc exerted a concentration-dependent dual effect on melanoma cells and that this effect involved modulation of the ERK-PTPN12-JAK2 axis. Specifically, low-dose Vc treatment promoted tumor progression, which was accompanied by activation of the ERK and JAK2 signaling pathways and inhibition of PTPN12 phosphatase activity. Conversely, high-dose Vc treatment resulted in antitumor effects, which were accompanied by the suppression of the ERK and JAK2 signaling pathways and the increase in PTPN12 activity. Mechanistically, ERK mediated the phosphorylation of PTPN12 at Ser^{434}, thereby regulating its phosphatase activity. JAK2 was further identified as a novel substrate of PTPN12, and its activity was negatively regulated by PTPN12.

Our data revealed that low-dose Vc treatment induced ERK activation in B16-F10 cells, whereas high-dose Vc treatment inhibited ERK activity (Figure 4D). We also observed this bidirectional regulation in HeLa cells (Supplementary Figure S4A), indicating that Vc modulates ERK activity in a concentration-dependent manner. ERK is overexpressed in more than 85% of cancers, and more than 40% of these cases exhibit sustained ERK

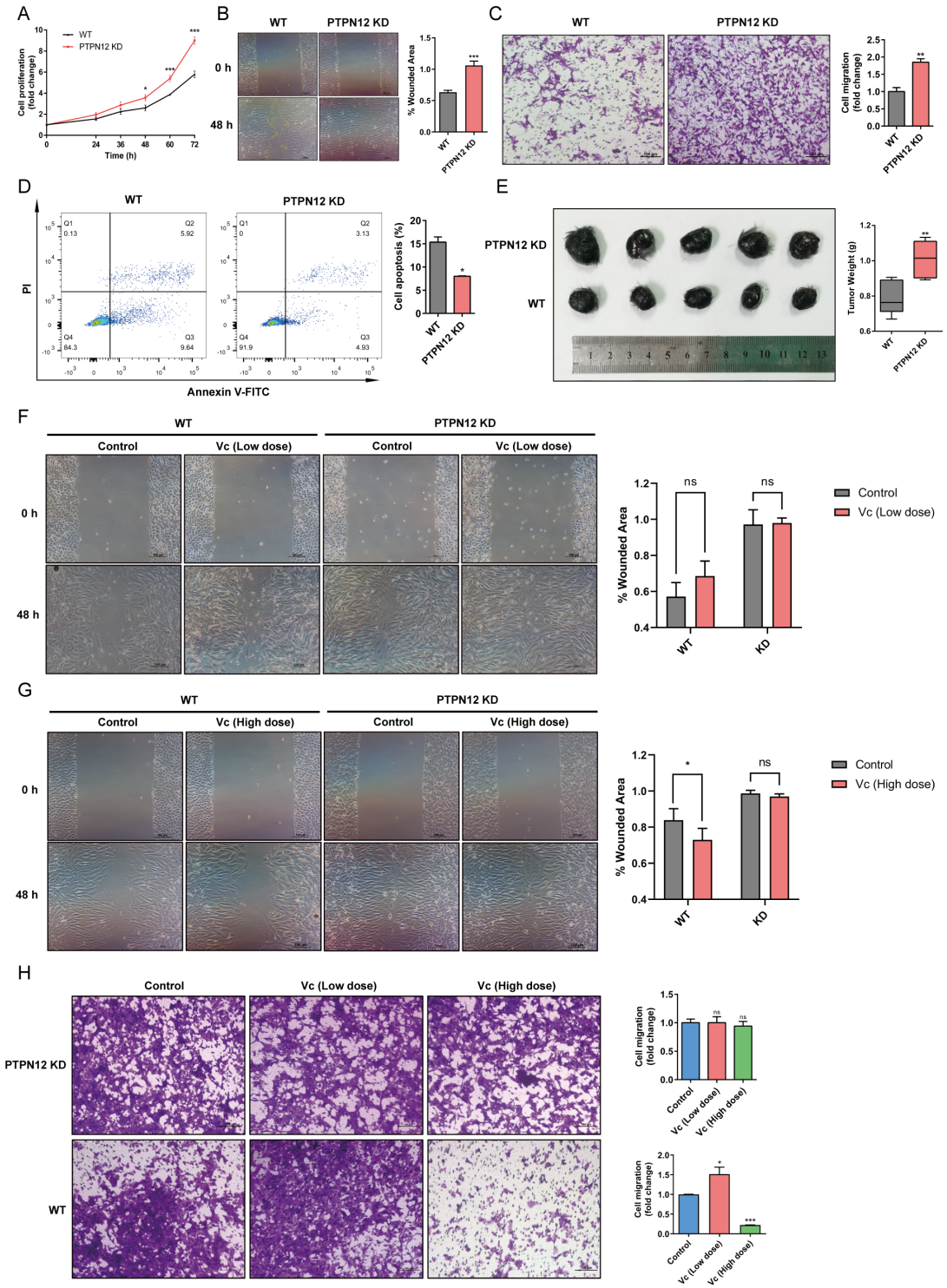


Figure 5. Knockdown of *Ptpn12* eliminates Vc-induced migration in melanoma cells (A) The proliferation of wild-type and *Ptpn12*-knockdown B16-F10 cells was evaluated by a CCK8 assay. (B,C) The migration ability of wild-type and *Ptpn12*-knockdown B16-F10 cells was detected by wound healing (B) and Transwell (C) assays. Scale bar, 100 μm. (D) The apoptosis of wild-type and *Ptpn12*-knockdown B16-F10 cells was detected by flow cytometry. (E) Effects of *Ptpn12* knockdown on xenograft tumor growth *in vivo*. Left: representative images of tumors in mouse models constructed from wild-type or *Ptpn12*-knockdown B16-F10 cells ($n = 5$). Right: tumor weight was measured after tumor excision. (F–H) The migration ability of wild-type and *Ptpn12*-knockdown B16-F10 cells treated with different doses of Vc was determined by wound healing assays (F,G) and Transwell assays (H). Scale bar, 100 μm. The low-dose Vc concentration was 10 μg/mL, and the high-dose Vc concentration was 500 μg/mL. Data are presented as the mean ± SD. Two-tailed Student's *t* test compared with the control. $^{*}P < 0.05$, $^{**}P < 0.01$, $^{***}P < 0.001$. ns, not significant.

activation because of mutations in BRAF and its upstream activator RAS, thereby driving tumor cell proliferation [23,24]. Previous studies have reported that low-dose Vc facilitates tumor growth in malignant melanoma and lung cancer [10,45], whereas high-dose Vc has cytotoxic effects on multiple tumor types, including ovarian, pancreatic, and colorectal cancers [46]. Collectively, our findings demonstrate that Vc bidirectionally regulates ERK activity to influence tumor progression.

Our findings indicate that Vc regulates the phosphatase activity of PTPN12 via ERK-mediated phosphorylation at Ser^{434}, thereby modulating JAK2 activity. SVCT2 functions as a receptor-like transporter to mediate 50 μg/mL Vc-induced JAK2 activation [16]. In this study, high-dose Vc suppressed JAK2 phosphorylation (Figure 2A), which is consistent with a recent report that Vc inhibits the JAK2/STAT3 pathway [47]. As a core kinase in the JAK-STAT signaling pathway, JAK2 with activating mutations (*e.g.*, V617F) or overexpression can drive tumor cell proliferation, invasion, metastasis, and immune evasion [48]. Thus, the suppression of JAK2 phosphorylation contributes to the antimelanoma effect of high-dose Vc. Notably, in myeloproliferative neoplasms (MPNs), where JAK2 V617F mutations are prevalent [49], resistance to JAK2 inhibitor therapy frequently occurs because of compensatory activation of the MAPK pathway, particularly that of ERK [50]. Importantly, high-dose Vc suppressed both JAK2 activity and ERK activity, highlighting its potential as a natural dual inhibitor of both JAK2 activity and ERK activity. This discovery suggests a potential strategy for overcoming resistance to targeted therapy in MPNs and melanoma while also helping to explain the enhanced antitumor effect of combining high-dose Vc with a JAK2 inhibitor (Figure 2B–E). Furthermore, high-dose Vc may exert antitumor effects through mechanisms beyond the JAK2 and ERK pathways, such as by suppressing the PI3K/AKT pathway and inducing oxidative stress.

This study demonstrated that knockdown of *Ptpn12* significantly promoted melanoma progression (Figure 5A–E). PTPN12 is a classical nonreceptor protein tyrosine phosphatase that functions as a tumor suppressor in multiple cancer types. For instance, in triple-negative breast cancer, the loss of PTPN12 leads to the aberrant activation of multiple receptor tyrosine kinases (RTKs), thereby promoting tumor growth [18]. Importantly, we found that low-dose Vc induces ERK activation, which in turn inhibits PTPN12 phosphatase activity by increasing its phosphorylation at Ser^{434}. These findings provide a potential explanation for how low-dose Vc promotes tumor growth. Conversely, high-dose Vc suppressed ERK activity, leading to reduced PTPN12 phosphorylation and increased PTPN12 phosphatase activity, which contributed to the antitumor effects of high-dose Vc. Previous studies have shown that kinases such as PKA, PKC, and PLK4 reduce PTPN12 activity through phosphorylation of Ser^{434} [21,51]. We identified ERK as a novel kinase targeting Ser^{434} and demonstrated that ERK1, but not ERK2 or MEK, specifically binds to and phosphorylates PTPN12 (Supplementary Figure S4B). These findings reveal a novel mechanism and specific site for ERK subtype-selective regulation of PTPN12, thereby providing new targets for precise intervention in related pathways. Furthermore, these discoveries further elucidate previous observations that ERK1/2 phosphorylates PTPN12 and enhances its interaction with focal adhesion kinase (FAK), thereby modulating FAK activity [22]. We provide the first evidence that PTPN12 directly binds to and dephosphorylates JAK2. Although known substrates of PTPN12 include AMPK, PPARα, and CDK2 [17,18,52], JAK2 has not previously been identified as a substrate. Other PTPN family members, such as PTPN1, PTPN2, and PTPN6, reportedly interact with JAK proteins and regulate the JAK/STAT pathway [14,15,36]. However, our protein interaction and substrate trapping assays demonstrated that JAK2 is a novel substrate of PTPN12. This represents a direct regulatory interaction between PTPN12 and JAK2, establishing a previously unknown link between this tumor suppressor and a key oncogenic kinase and thereby expanding the known substrate repertoire of PTPN12. Thus, PTPN12 may exert its antitumor effects by attenuating JAK2 activity, which is consistent with our observation that high-dose Vc inhibits JAK2 activity.

A previous study reported that Vc-mediated vicinylation of STAT1 at K298 impaired its interaction with the phosphatase PTPN2, thereby enhancing STAT1-mediated IFN pathway activation in tumor cells [53]. In our study, the ERK-PTPN12-JAK2 axis highlights the pivotal role of PTPN12 in bridging upstream ERK signaling and downstream JAK2 activity. We further observed that low-dose Vc had a more pronounced effect on melanoma cell chemotactic migration than on cell proliferation or apoptosis. Additionally, knockdown of *Ptpn12* substantially abolished the regulatory effect of Vc on melanoma cell migration, indicating that the effect is independent of the dose of Vc. These results indicate that Vc modulates tumor migration primarily by targeting PTPN12.

In this study, we observed a concentration-dependent dual effect of Vc on melanoma: low-dose Vc promoted tumor cell chemotactic migration and accelerated tumor progression, whereas high-dose Vc induced cytotoxicity and exerted antitumor activity. This finding mirrors the dual effects reported for the classic chemotherapeutic agent 5-fluorouracil (5-FU) [54,55]. The dual role of Vc has also been confirmed in previous studies, where low-dose Vc facilitates tumor growth by activating the BRAF, AKT and BACH1 proteins [10,45]. In contrast, high-dose Vc exerts antitumor effects through multiple mechanisms, including reactive oxygen species (ROS)-mediated cytotoxicity, suppression of the MAPK/ERK and PI3K/AKT pathways, and enhancement of STAT1-mediated immune responses via lysineylation [10,26,53]. The ERK-PTPN12-JAK2 axis identified in our study further enriched the signaling pathways associated with Vc and elucidated the molecular mechanisms underlying its concentration-dependent dual effects on melanoma.

Pharmacokinetic studies have indicated that intravenous administration of 3 g of Vc can achieve plasma concentrations exceeding 500 μg/mL without significant toxicity [5]. Importantly, our study demonstrated that 500 μg/mL Vc is sufficient to kill melanoma cells. Several clinical trials have further confirmed that high-dose intravenous Vc can improve quality of life and prolong overall survival in patients with advanced cancer [56,57]. Collectively, our findings support the potential of high-dose intravenous Vc as a safe and effective adjunctive therapy for melanoma. However, the present study also revealed that low-dose Vc, which corresponds to plasma concentrations achieved by conventional oral supplementation (typically in the micromolar range, far below the cytotoxic threshold of 500 μg/mL), might paradoxically promote melanoma progression. These findings suggest that routine oral Vc supplementation should be approached with caution in melanoma patients. This finding also highlights the critical importance of optimizing the administration route and dosage in the context of Vc-based cancer therapies.

Our mechanistic investigations were performed primarily using

the murine melanoma cell line B16-F10 and derived xenograft models. Further validation in additional melanoma cell lines and patient samples will strengthen the clinical relevance of our findings. Additionally, while the results of this study demonstrate that inhibiting JAK2 activity is a key event in the antitumor effects of high-dose Vc and that pharmacological inhibition of JAK2 can recapitulate these effects, future rescue experiments using JAK2 gain-of-function mutation models are needed to conclusively demonstrate the necessity of this pathway.

In summary, this study revealed a concentration-dependent mechanism through which Vc regulates melanoma progression through the ERK-PTPN12-JAK2 axis. Our data support a model in which low-dose Vc promotes melanoma progression via this axis, whereas high-dose Vc at millimolar concentrations exerts antitumor effects, at least in part, through the same axis. Importantly, several clinical trials have reported no significant toxicity when intravenous administration of high-dose Vc achieves effective plasma concentrations in the millimolar range. Given its low cost and favorable safety profile, high-dose Vc is a promising adjunct approach that requires further preclinical validation. Future studies should explore the combined effects of high-dose Vc with existing targeted therapies or immunotherapies, particularly to overcome resistance mechanisms driven by ERK or JAK2 signaling. However, melanoma patients should exercise greater caution when they are taking oral vitamin C supplements.

Supplementary Data

Supplementary data are available at *Acta Biochimica et Biophysica Sinica* online.

Data Availability

Data can be accessed upon reasonable request from the corresponding author.Conceptualization, Z.G.; Methodology, C.Z. and B.C.; Validation, W.H., Y.L. and H.W.; Investigation, S.X. and Y.G.; Resources, S.J.; Writing—Original Draft Preparation, C.Z.; Writing—Review and Editing, C.Z.; Project Administration, Z.G.; Software, C.Z. and S.J.; Funding Acquisition, Z.G. All authors have read and agreed to the published version of the manuscript.

Funding

This work was supported by the grants from the National Natural Science Foundation of China (Nos. 32150002 and 31572405).

Conflict of Interest

The authors declare that they have no conflict of interest.

References

1. Kobayashi TA, Shimada H, Sano FK, Itoh Y, Enoki S, Okada Y, Kusakizako T, *et al.* Dimeric transport mechanism of human vitamin C transporter SVCT1. *Nat Commun* 2024, 15: 5569
2. Cameron E, Pauling L. The orthomolecular treatment of cancer. I. The role of ascorbic acid in host resistance. *Chem Biol Interact* 1974, 9: 273–283
3. Creagan ET, Moertel CG, O'Fallon JR, Schutt AJ, O'Connell MJ, Rubin J, Frytak S. Failure of high-dose vitamin C (ascorbic acid) therapy to benefit patients with advanced cancer. *N Engl J Med* 1979, 301: 687–690
4. Moertel CG, Fleming TR, Creagan ET, Rubin J, O'Connell MJ, Ames MM. High-dose vitamin C versus placebo in the treatment of patients with advanced cancer who have had no prior chemotherapy. *N Engl J Med* 1985, 312: 137–141
5. Padayatty SJ, Sun H, Wang Y, Riordan HD, Hewitt SM, Katz A, Wesley RA, *et al.* Vitamin C pharmacokinetics: implications for oral and intravenous use. *Ann Intern Med* 2004, 140: 533–537
6. Yun J, Mullarky E, Lu C, Bosch KN, Kavalier A, Rivera K, Roper J, *et al.* Vitamin C selectively kills *KRAS* and *BRAF* mutant colorectal cancer cells by targeting GAPDH. *Science* 2015, 350: 1391–1396
7. Sun X, Cai X, Li S, Pi R, Guo Z, Jiang J, Wang P, *et al.* High-dose ascorbic acid selectively induces pyroptosis in LKB1-deficient lung cancer and sensitizes immunotherapy. *Cell Rep Med* 2025, 6: 102291
8. Ferrada L, Magdalena R, Barahona MJ, Ramírez E, Sanzana C, Gutiérrez J, Nualart F. Two distinct faces of vitamin C: AA vs DHA. *Antioxidants* 2021, 10: 215
9. Sayin VI, Ibrahim MX, Larsson E, Nilsson JA, Lindahl P, Bergo MO. Antioxidants accelerate lung cancer progression in mice. *Sci Transl Med* 2014, 6: 221ra15
10. Yang G, Yan Y, Ma Y, Yang Y. Vitamin C at high concentrations induces cytotoxicity in malignant melanoma but promotes tumor growth at low concentrations. *Mol Carcinog* 2017, 56: 1965–1976
11. Ou A, Ott M, Fang D, Heimberger A. The role and therapeutic targeting of JAK/STAT signaling in glioblastoma. *Cancers* 2021, 13: 437
12. Bertulfo K, Debackere K, Miller H, Najac R, Ma C, Ferrando AA, Palomero T. Therapeutic targeting of JAK/STAT signaling and histone acetyltransferase activity in post-myeloproliferative neoplasm secondary AML. *Blood* 2023, 142: 2792
13. Quelle FW, Wang J, Feng J, Wang D, Cleveland JL, Ihle JN, Zambetti GP. Cytokine rescue of p53-dependent apoptosis and cell cycle arrest is mediated by distinct Jak kinase signaling pathways. *Genes Dev* 1998, 12: 1099–1107
14. Sun R, Wei S, Yu Y, Wang Z, Yao T, Zhang Y, Cui L, *et al.* Prognostic value and immune infiltration of a tumor microenvironment-related PTPN6 in metastatic melanoma. *Cancer Cell Int* 2024, 24: 435
15. Baumgartner CK, Ebrahimi-Nik H, Iracheta-Vellve A, Hamel KM, Olander KE, Davis TGR, McGuire KA, *et al.* The PTPN2/PTPN1 inhibitor ABBV-CLS-484 unleashes potent anti-tumour immunity. *Nature* 2023, 622: 850–862
16. Han Z, Zhang Z, Guan Y, Chen B, Yu M, Zhang L, Fang J, *et al.* New insights into vitamin C function: vitamin C induces JAK2 activation through its receptor-like transporter SVCT2. *Int J Biol Macromol* 2021, 173: 379–398
17. Cao Y, Zheng Y, Niu R, Wang T, Yu H, Tong Y, Tang YD, *et al.* DUSP14 suppresses ferroptosis and promotes tumor progression of triple-negative breast cancer. *Cell Rep* 2025, 44: 116365
18. Neill NJ, Satpathy S, Krug K, Meena JK, Ramesh Babu N, Calderon C, Reed D, *et al.* Integrative proteogenomics and forward genetics reveal a novel mitotic vulnerability in triple-negative breast cancer. *Cancer Discov* 2025, 15: 2326–2343
19. Nakamura K, Palmer HEF, Ozawa T, Mashima K. Protein phosphatase 1 associates with protein tyrosine phosphatase-PEST inducing dephosphorylation of phospho-serine 39. *J Biochem* 2010, 147: 493–500
20. Li H, Yang D, Ning S, Xu Y, Yang F, Yin R, Feng T, *et al.* Switching of the substrate specificity of protein tyrosine phosphatase N12 by cyclin-dependent kinase 2 phosphorylation orchestrating 2 oncogenic pathways. *FASEB J* 2018, 32: 73–82
21. Byrne DP, Clarke CJ, Brownridge PJ, Kalyuzhnyy A, Perkins S, Campbell A, Mason D, *et al.* Use of the polo-like kinase 4 (PLK4) inhibitor centrinone to investigate intracellular signalling networks using SILAC-based phosphoproteomics. *Biochem J* 2020, 477: 2451–2475
22. Zheng Y, Yang W, Xia Y, Hawke D, Liu DX, Lu Z. Ras-induced and extracellular signal-regulated kinase 1 and 2 phosphorylation-dependent isomerization of protein tyrosine phosphatase (PTP)-PEST by PIN1

promotes FAK dephosphorylation by PTP-PEST. *Mol Cell Biol* 2011, 31: 4258–4269
23. Yuan J, Dong X, Yap J, Hu J. The MAPK and AMPK signalings: interplay and implication in targeted cancer therapy. *J Hematol Oncol* 2020, 13: 113
24. Barbosa R, Acevedo LA, Marmorstein R. The MEK/ERK network as a therapeutic target in human cancer. *Mol Cancer Res* 2021, 19: 361–374
25. Yan Y, Zeng W, Song S, Zhang F, He W, Liang W, Niu Z. Vitamin C induces periodontal ligament progenitor cell differentiation via activation of ERK pathway mediated by PELP1. *Protein Cell* 2013, 4: 620–627
26. Su X, Shen Z, Yang Q, Sui F, Pu J, Ma J, Ma S, ***et al.*** Vitamin C kills thyroid cancer cells through ROS-dependent inhibition of MAPK/ERK and PI3K/AKT pathways via distinct mechanisms. *Theranostics* 2019, 9: 4461–4473
27. Liu Y, Wei X, Zhang C, Liu J, Yu M, Feng P, Guo Z. PGC7 maintains the pluripotency of F9 embryonic carcinoma cells by promoting Nanog translation. *Acta Biochim Biophys Sin* 2025, 57: 1469–1480
28. Liu Y, Ren X, Ke J, Zhang Y, Wei Q, Shi Z, Ai Z, ***et al.*** SC1 inhibits the differentiation of F9 embryonic carcinoma cells induced by retinoic acid. *Acta Biochim Biophys Sin* 2018, 50: 793–799
29. Liang L, Xu C, Wang Y, Feng Y, Jia W, Wang J, Zhao W, ***et al.*** GALNT7 promotes hepatocellular carcinoma progression by activating the PI3K/AKT signaling pathway via O-glycosylation of MUC13. *Acta Biochim Biophys Sin* 2025, 58: 322–336
30. Yu M, Liu Y, Han Z, Du W, Chen B, Zhang L, Xue H, ***et al.*** Involvement of PGC7 and UHRF1 in the regulation of DNA methylation of the IG-DMR in the imprinted *Dlk1-Dio3* locus. *Acta Biochim Biophys Sin* 2022, 54: 917–930
31. Lam AJ, St-Pierre F, Gong Y, Marshall JD, Cranfill PJ, Baird MA, McKeown MR, ***et al.*** Improving FRET dynamic range with bright green and red fluorescent proteins. *Nat Methods* 2012, 9: 1005–1012
32. Xia Z, Liu Y. Reliable and global measurement of fluorescence resonance energy transfer using fluorescence microscopes. *Biophys J* 2001, 81: 2395–2402
33. Streit S, Ruhe JE, Knyazev P, Knyazeva T, Iacobelli S, Peter S, Hoefler H, ***et al.*** PTP-PEST phosphatase variations in human cancer. *Cancer Genet CytoGenet* 2006, 170: 48–53
34. Stephenson CM, Levin RD, Spector T, Lis CG. Phase I clinical trial to evaluate the safety, tolerability, and pharmacokinetics of high-dose intravenous ascorbic acid in patients with advanced cancer. *Cancer Chemother Pharmacol* 2013, 72: 139–146
35. Wang F, He MM, Xiao J, Zhang YQ, Yuan XL, Fang WJ, Zhang Y, ***et al.*** A randomized, open-label, multicenter, phase 3 study of high-dose vitamin C plus FOLFOX ± bevacizumab versus FOLFOX ± bevacizumab in unresectable untreated metastatic colorectal cancer (VITALITY Study). *Clin Cancer Res* 2022, 28: 4232–4239
36. Huang TT, Su JC, Liu CY, Shiau CW, Chen KF. Alteration of SHP-1/p-STAT3 signaling: a potential target for anticancer therapy. *Int J Mol Sci* 2017, 18: 1234
37. Salazar K, Martínez M, Ulloa V, Bertinat R, Martínez F, Jara N, Espinoza F, ***et al.*** SVCT2 overexpression in neuroblastoma cells induces cellular branching that is associated with ERK signaling. *Mol Neurobiol* 2016, 53: 6668–6679
38. Garton AJ, Tonks NK. PTP-PEST: a protein tyrosine phosphatase regulated by serine phosphorylation. *EMBO J* 1994, 13: 3763–3771
39. Andersen JN, Mortensen OH, Peters GH, Drake PG, Iversen LF, Olsen OH, Jansen PG, ***et al.*** Structural and evolutionary relationships among protein tyrosine phosphatase domains. *Mol Cell Biol* 2001, 21: 7117–7136
40. Perla S, Qiu B, Dorry S, Yi JS, Bennett AM. Identification of protein tyrosine phosphatase (PTP) substrates. *Methods Mol Biol* 2024, 2743: 123-133
41. Koroknai V, Ecsedi S, Vízkeleti L, Kiss T, Szász I, Lukács A, Papp O, ***et al.*** Genomic profiling of invasive melanoma cell lines by array comparative genomic hybridization. *Melanoma Res* 2016, 26: 100–107
42. Chen Z, Morales JE, Guerrero PA, Sun H, McCarty JH. PTPN12/PTP-PEST regulates phosphorylation-dependent ubiquitination and stability of focal adhesion substrates in invasive glioblastoma cells. *Cancer Res* 2018, 78: 3809–3822
43. Huo Y, Wang Y, Meng L, Zhang A, Liu B. Progress in the correlation between PTPN12 gene expression and human tumors. *Medicine* 2020, 99: e20445
44. Lee C, Rhee I. Important roles of protein tyrosine phosphatase PTPN12 in tumor progression. *Pharmacol Res* 2019, 144: 73–78
45. Wang T, Dong Y, Huang Z, Zhang G, Zhao Y, Yao H, Hu J, ***et al.*** Antioxidants stimulate BACH1-dependent tumor angiogenesis. *J Clin Invest* 2023, 133: e169671
46. Zhao H, Fu W, Yang X, Zhang W, Wu S, Ma J, Zhang T, ***et al.*** High-dose vitamin C: a promising anti-tumor agent, insight from mechanisms, clinical research, and challenges. *Genes Dis* 2026, 13: 101742
47. Han RD, Tian N, Sun ZG, Liu AB, Wang S, Shen Y, Liu J, ***et al.*** Vitamin C protects against myocardial damage induced by sepsis by regulating the JAK2/STAT3 and NF-κB signaling pathways. *J Surg Res* 2025, 314: 209–219
48. Zhang Y, Zhao Y, Liu Y, Zhang M, Zhang J. New advances in the role of *JAK2* V617F mutation in myeloproliferative neoplasms. *Cancer* 2024, 130: 4229–4240
49. Stewart BL, Carraway HE, Alvarez AL, Lesmana H, Molina J, Tu ZJ, Bosler DS, ***et al.*** *JAK2* p.R564 germ line variants associated with hereditary thrombocythemia and hematologic neoplasms. *Blood Adv* 2025, 9: 1534–1543
50. Brkic S, Stivala S, Santopolo A, Szybinski J, Jungius S, Passweg JR, Tsakiris D, ***et al.*** Dual targeting of JAK2 and ERK interferes with the myeloproliferative neoplasm clone and enhances therapeutic efficacy. *Leukemia* 2021, 35: 2875–2884
51. Habib T, Herrera R, Decker SJ. Activators of protein kinase C stimulate association of Shc and the PEST tyrosine phosphatase. *J Biol Chem* 1994, 269: 25243–25246
52. Chandel S, Manikandan A, Mehta N, Nathan AA, Tiwari RK, Mohapatra SB, Chandran M, ***et al.*** The protein tyrosine phosphatase PTP-PEST mediates hypoxia-induced endothelial autophagy and angiogenesis via AMPK activation. *J Cell Sci* 2021, 134: jcs250274
53. He XD, Wei Y, Wu J, Wang QW, Bergholz JS, Gu H, Zou JJ, ***et al.*** Lysine vitcylation is a novel vitamin C-derived protein modification that enhances STAT1-mediated immune response. *bioRxiv* 2023: 2023.06.27.546774
54. Chen JK, Merrick KA, Kong YW, Izrael-Tomasevic A, Eng G, Handly ED, Patterson JC, ***et al.*** An RNA damage response network mediates the lethality of 5-FU in colorectal cancer. *Cell Rep Med* 2024, 5: 101778
55. You H, Zhao P, Zhao X, Zheng Q, Ma W, Cheng K, Li M, ***et al.*** Promotion of tumor angiogenesis and growth induced by low-dose antineoplastic agents via bone-marrow-derived cells in tumor tissues. *Front Pharmacol* 2024, 15: 1414832
56. Böttger F, Vallés-Martí A, Cahn L, Jimenez CR. High-dose intravenous vitamin C, a promising multi-targeting agent in the treatment of cancer. *J Exp Clin Cancer Res* 2021, 40: 343
57. Cenigaonandia-Campillo A, Garcia-Bautista A, Rio-Vilariño A, Cebrian A, del Puerto L, Pellicer JA, Gabaldón JA, ***et al.*** Vitamin-C-dependent downregulation of the citrate metabolism pathway potentiates pancreatic ductal adenocarcinoma growth arrest. *Mol Oncol* 2024: 1878-0261.13616